HHS Public Access

Author manuscript

Clin Cancer Res. Author manuscript; available in PMC 2024 July 17.

Published in final edited form as:

Clin Cancer Res. 2024 January 17; 30(2): 283–293. doi:10.1158/1078-0432.CCR-22-3952.

Magnetic resonance imaging of iron metabolism with T_2* mapping predicts an enhanced clinical response to pharmacological ascorbate in patients with GBM

Michael S. Petronek[1], **Varun Monga**[2], **Kellie L. Bodeker**[1], **Michael Kwofie**[3], **Chu-Yu Lee**[3], **Kranti A. Mapuskar**[1], **Jeffrey M. Stolwijk**[1], **Amira Zaher**[1], **Brett A. Wagner**[1], **Mark C. Smith**[1], **Sandy Vollstedt**[1], **Heather Brown**[1], **Meghan L. Chandler**[1], **Amanda C. Lorack**[1], **Jared S. Wulfekuhle**[1], **Jann N. Sarkaria**[4], **Ryan T. Flynn**[1], **Jeremy D.W. Greenlee**[5], **Matthew A. Howard**[5], **Brian J. Smith**[6], **Karra A. Jones**[7], **Garry R. Buettner**[1], **Joseph J. Cullen**[8], **Joel St-Aubin**[1], **John M. Buatti**[1], **Vincent A. Magnotta**[3], **Douglas R. Spitz**[1,*], **Bryan G. Allen**[1,*]

[1]Department of Radiation Oncology, University of Iowa; Iowa City, IA, USA

[2]Department of Internal Medicine, Division of Hematology and Oncology, University of Iowa; Iowa City, IA, USA

[3]Department of Radiology, University of Iowa; Iowa City, IA, USA

[4]Department of Radiation Oncology, Mayo Clinic; Rochester, MN, USA

[5]Department of Neurosurgery, University of Iowa; Iowa City, IA, USA

[6]Department of Biostatistics, University of Iowa; Iowa City, IA, USA

[7]Department of Pathology, Division of Neuropathology, Duke University; Durham, NC, USA

[8]Department of Surgery, University of Iowa; Iowa City, IA, USA

Abstract

Purpose: Pharmacological ascorbate ($P\text{-}AscH^-$) is hypothesized to be an Fe-dependent tumor-specific adjuvant to chemo-radiation in treating glioblastoma (GBM). The current study determined the efficacy of combining $P\text{-}AscH^-$ with radiation and temozolomide in a phase 2 clinical trial while simultaneously investigating a mechanism-based, non-invasive biomarker in T_2* mapping to predict GBM response to $P\text{-}AscH^-$ in humans.

Patients and Methods: The single-arm phase 2 clinical trial (NCT02344355) enrolled 55 subjects with analysis performed 12 months following the completion of treatment. Overall survival (OS) and progression-free survival (PFS) were estimated with the Kaplan-Meier method

Address all correspondence to: Bryan G. Allen, MD PhD MBA, Free Radical and Radiation Biology, Department of Radiation Oncology, Holden Comprehensive Cancer Center, University of Iowa Hospitals and Clinics, Iowa City, IA 52242, Tel: (319) 356-8019 (secretary), Fax: (319) 335-8039, bryan-allen@uiowa.edu; Douglas R. Spitz, PhD, Free Radical and Radiation Biology, Department of Radiation Oncology, Holden Comprehensive Cancer Center, University of Iowa Hospitals and Clinics, Iowa City, IA 52242, douglas-spitz@uiowa.edu.

*-These authors made equal contributions to the manuscript

Conflicts of interest: The authors declare no conflict of interest.

and compared across patient subgroups with log-rank tests. 49 of 55 subjects were evaluated using T_2*-based MRI to assess its utility as an Fe-dependent biomarker.

Results: Median OS was estimated to be 19.6 months (90% CI: 15.7 – 26.5 months), a statistically significant increase compared to historic control patients (14.6 months). Subjects with initial T_2* relaxation < 50 ms were associated with a significant increase in PFS compared to T_2*_{high} subjects (11.2 months vs. 5.7 months, $p<0.05$) and a trend towards increased OS (26.5 months vs. 17.5 months). These results were validated in pre-clinical *in vitro* and *in vivo* model systems.

Conclusions: P-AscH$^-$ combined with temozolomide and radiotherapy has the potential to significantly enhance GBM survival. T_2*-based MRI assessment of tumor iron content is a prognostic biomarker for GBM clinical outcomes.

Introduction

Glioblastoma (GBM) is the most common primary brain malignancy with an incidence of ≈14,000 cases per year, median overall survival of 14–16 months, and 5-year overall survival (OS) <10% when treated with standard radiation and temozolomide (SOC) (1–3). GBM tumors have significant increases in transferrin receptors (TfR) and ferritin heavy chains (FtH) (4). The presumed result of these alterations is increased GBM iron (Fe) content compared to non-malignant brain tissues. The increasingly available Fe contributes to the intracellular labile iron pool (LIP), redox active Fe that is chelatable(5). The LIP makes up <5% of the total Fe within cells and is comprised primarily of ferrous (Fe^{2+}) iron (6,7). Despite being a small portion of the total Fe content within the cell, the LIP is the central hub of iron metabolism (8). The LIP is tightly regulated within the cell because redox active Fe may facilitate the formation of reactive oxygen species (ROS) by Fenton chemistry generating oxidative damage and genomic instability (9),(10). Because of Fe metabolic differences in tumor versus non-malignant tissues, several therapies are under investigation to target tumor Fe metabolism.(11)

A promising anti-cancer therapy that depends upon Fe metabolism is pharmacological ascorbate (P-AscH$^-$; plasma [ascorbate] ~20 mM). P-AscH$^-$ exhibits GBM-specific anti-cancer activites *in vitro*, in xenograft models, and in a phase I clinical trial when combined with radiation and temozolomide(12). Chemically, AscH$^-$ is a reducing agent that converts Fe^{3+} to Fe^{2+} and can facilitate the release of Fe from proteins such as ferritin (13,14). In this way, P-AscH$^-$ can effectively increase the intracellular LIP in GBM cells (12,15). P-AscH$^-$'s GBM cytotoxicty is through increased $O_2^{\bullet -}$ and H_2O_2 production facilitated by the reduction of Fe^{3+} to Fe^{2+} (12). Therefore, a non-invasive, *in vivo* method of measuring the reduction of Fe may provide a novel tool for assessing P-AscH$^-$ treatment efficacy.

T_2* mapping is an MRI technique that can detect tissue Fe content. Clinically, T_2* mapping has been adopted to evaluate Fe overload in heart and liver tissues (16–22). T_2* relaxation times are inversely proportional to Fe content(23–25). However, this work has illuminated that T_2* mapping exhibits Fe oxidation state specificity due to proton-electron dipole-dipole interactions (26). Thus, it is hypothesized that P-AscH$^-$ cytotoxicity resulting from redox-mediated disruption of iron (Fe) metabolism can be non-invasively detected using T_2* MRI

to evaluate patient outcomes (27). The current study determined the efficacy of combining P-AscH$^-$ with radiation and temozolomide in a phase II clinical trial while simultaneously developing a mechanism-based, non-invasive biomarker in T_2* mapping to predict GBM response to P-AscH$^-$ in humans.

Materials and Methods

Cell culture

All glioma cells (U87, ATCC HTB-14; U251 Millipore Sigma, 09063001) were cultured in DMEM-F12 media (15% FBS, 1% penicillin-strep, 1% Na-pyruvate, 1.5% HEPES, 0.1% insulin, and 0.02% fibroblast growth factor) and grown to 70 – 80% confluence at 21% O_2 before experimentation. Patient-derived glioblastoma cells (GBM06 is a primary GBM from a male donor, GBM76 is a recurrent GBM from a male donor) were a gift from Dr. Jann Sarkaria, MD (Mayo Clinic, Rochester, Mn). All cells were confirmed to be mycoplasma negative by the University of Iowa Genomics Core prior to use. Commercial cells were used for up to 15 passages and patient-derived cells were used for up to 10 passages.

U251 FtH+ cells were generated using a ferritin heavy chain-pTRIPZ vector and transduced using the protocol previously described.(28) FtH overexpression was achieved using lentiviral transduction of a ferritin heavy chain-pTRIPZ vector. Lentivirus was generated in TSA201 cells along with VSV-G (RRID:Addgene_138479) and psPAX2 helper vectors (RRID:Addgene_12260). Virus was collected from TSA201 cell cultures, centrifuged to remove cell debris, and filtered using 0.45 μm filters from the ZymoPUREtm II Plasmid Midiprep Kit (Zymo Research, Irvine CA, USA). U251 cells were plated and allowed to grow for 24 h, and virus was then added to the cells with 8 μg/mL of polybrene for a total of 48 h. Fresh virus was added after 24 h. Following transduction, cells were selected with 2.5 μg/mL puromycin. For experiments using a doxycycline-inducible FtH overexpressing model, cells were treated with 1 μg mL^{-1} doxycycline daily for the appropriate time. Human holo-transferrin (T0665, Sigma-Aldrich; St. Louis, MO) was diluted in double-distilled H_2O in 10 mg mL^{-1} stocks and stored a 4 °C until use. Cells cultures were supplemented with holo-transferrin at 200 μg mL^{-1} for the equivalent time as doxycycline (48 h). For clonogenic survival analysis, cells were plated as a single-cell monolayer and allowed to incubate for 7–14 days before staining with Coomassie blue for colony counting.

Detection of labile iron with UV-Visible light spectroscopy

Measurement of labile Fe^{2+} was accomplished using the ferrozine assay.(29) Recombinant ferritin (1.1 mM) from equine spleen (Sigma-Aldrich, F4503) was diluted in distilled H_2O at room temperature and incubated for 24 h with 300 mM AscH$^-$. Stocks were diluted at 1:15 in a 1x PBS (pH = 6.5) buffer with 5 mM ferrozine. [Fe^{2+}] using ε_{562} = 27,900 M^{-1} cm^{-1}.

Labile iron concentrations in tissue samples were determined using a ferrozine-based colorimetric assay as previously described by Abbasi *et al.*(30) Tissue samples were homogenized in 1X RIPA lysis buffer (Sigma-Aldrich; R0278). Cell debris was removed by centrifugation at maximum speed (14,000 g) for 10 min. 100 μL of the supernatant was then diluted with 100 μL ferrozine buffer (5 mM ferrozine, 1.25 M ammonium acetate, 10

mM ascorbate) in a single well of a clear 96 well plate. Following dilution, the 96-well plate was evaluated for the formation of a Fe^{2+}-ferrozine complex by monitoring the absorbance at 562 nm and Fe concentration was calculated using Beer's Law with pathlength for 200 μL ≈ 0.55 cm and ε_{562} = 27,900 M^{-1} cm^{-1}.

Western blotting

Exponentially growing cells were washed with PBS before the addition of lysis buffer (Cell Signaling), incubated on ice for 5 min, scraped, and sonicated 3× 10 s. The lysate was centrifuged to remove cellular debris. The protein concentrations were determined on the cleared lysate using the Bio-Rad DC Bradford Protein Assay (Bio-Rad Laboratories, RRID:SCR_008426; Hercules, CA. Total protein (25 μg) was electrophoresed on a 4–20% gradient gel (Bio-Rad) at 80 V for approximately 1 h. The separated proteins were transferred onto PVDF membrane (Millipore, Billerica, CA) and non-specific binding was blocked using 5% nonfat dry milk in PBS-Tween (0.2%) for 1 hr at room temperature. The membranes were incubated with primary antibodies (Ferritin heavy chain (1:1000), Abcam, Cambridge, MA; Transferrin receptor, 1:1000, Invitrogen, Camarillo, CA) at 4° C overnight. B-tubulin was used as a loading control (1:4,000; Sigma-Aldrich). Following 3× 5 min PBS-Tween washes, the membranes were blotted with secondary antibodies (1:25,000; Sigma-Aldrich, St. Louis, MO) that were conjugated with horseradish peroxidase for 1 h. The washed membranes were incubated with Super Signal West Pico Chemiluminescent Substrate (Thermo Scientific, Rockford, IL) and exposed to Carestream BioMax MR Film (Carestream Health, Rochester, NY).

Aconitase Activity

Exponentially growing cells were scraped and frozen as dry pellets until assayed for total aconitase activity adapted from as previously described(31). Briefly, cell pellets were resuspended in 50 mM Tris-HCl, pH 7.4 with 0.6 mM $MnCl_2$ and 5 mM Na-citrate and sonicated 3× 10 s each. Protein was quantified by the Lowry method.(32) Aconitase activity was measured as the rate of appearance of NADPH (at 340 nm; Beckman DU 800 spectrophotometer, Brea, CA) for 45 min during the reaction of 200 μg total sample protein with 200 μM $NADP^+$ and 10 U isocitrate dehydrogenase.

Labile iron pool measures with flow cytometry

Intracellular labile iron pool measures were performed using a Calcein-AM fluorescent dye as previously described by Schoenfeld *et al.* (12) After cell harvesting, cell pellets were washed in PBS, then resuspended at approximately 1 × 10^6 cells mL^{-1} in 500 nM Calcein-AM in PBS. Samples were incubated for 15 min at 4% O_2 (37 °C, 5% CO_2). Following incubation, extracellular Calcein-AM was removed by washing with PBS, and cells were resuspended in 1 mL PBS before dividing each sample into two flow cytometry sample tubes. One of the two tubes was treated with 100 μM 2′,2′-bipyridyl (BIP) to chelate Fe away from Calcein and restore fluorescence. Samples were kept at room temperature for at least 15 min to allow full chelation of labile Fe by BIP. Following incubation 10,000 cells were analyzed on an LSR II Flow Cytometer (BD Biosciences, RRID:SCR_013311; λ_{ex} = 488 nm, λ_{em} = 515/20 nm). The LIP was quantified using the following formula:

$$\mathrm{LIP(A.U.)} = \mathrm{MFI_{BIP+}} - \mathrm{MFI_{BIP-}}$$

Treated samples were normalized against the control samples to calculate the relative labile iron pool.

Orthotopic mouse injections

Before injection, cells were trypsinized and the pellet was resuspended in 5% methylcellulose. Female nude athymic (NU/J) mice (Jackson Labs, RRID:IMSR_JAX:002019) were anesthetized using a ketamine (87.5 mg mL^{-1}) xylazine (12.5 mg mL^{-1}) cocktail by the University of Iowa IACUC. Following anesthesia, a 1 cm incision was made to expose the skull and a burr hole was made approximately 3 mm lateral (right) and 2 mm posterior to the bregma. A syringe containing cell + 5% methylcellulose was inserted 3 mm deep to the burr hole and 6×10^5 cells in 4 μL were injected over 1 min. Following completion of the surgery, mice received a 5-day treatment of meloxicam (2 mg kg^{-1}) for pain management. For U87 cells transfected with luciferase, tumor formation was confirmed by bioluminescence imaging using an Invitrogen IVIS system 10 min following injection of a Luciferin substrate (0.375 mg kg^{-1}; Pierce's D-luciferin, Thermo Fischer Scientific, 88291). Following MR confirmation of tumors as a hyperintense region on a T_2-weighted anatomical image, mice were treated with intraperitoneal $AscH^-$ (4 g kg^{-1} twice daily) for up to 10 days. A preliminary group of tumors post-euthanasia was validated using Hematoxylin and Eosin staining and confirmed by a board-certified neuropathologist.

MRI Measurements

Pre-clinical—T_2* maps were generated by fitting each voxel to a mono-exponential curve using an in-house python code. For image registration, subsequent T_2-weighted anatomical images were aligned to the initial T_2-anatomical image with the linear transformation matrix being applied to the associated T_2* map using Advanced Normalization Tools (ANTs) software. Images were imported to Slicer3D software where regions of interest (ROIs) were delineated and mean T_2* values were calculated using the label statistics tool within 3D Slicer. For tumor volume measures, initial tumor volumes were determined using a T_2-weighted images. Following baseline tumor volume calculation, animals were randomized and treated with a singled fraction of 12 Gy WBRT using a Xstral Small Animal Radiation Research Platform with a single dose of temozolomide (2.5 mg kg^{-1} delivered intraperitoneally) ± daily P-$AscH^{-1}$ (4 g kg^{-1} delivered intraperitoneally). Tumor volumes were then calculated on day 7 using a T_2-weighted MR scan.

For therapeutic response analysis, tumors were confirmed prior to the beginning of treatment and baseline tumor volumes were calculated using a T_2-weighted anatomical image. Following tumor confirmation, tumor bearing mice were treated with SOC (12 Gy x 1 fraction radiation + 1 × 2.5 mg kg^{-1} TMZ) ± daily 4 g kg^{-1} P-$AscH^-$ for 7 days. At day 7, follow-up tumor volumes were again calculated using T_2-weighted anatomical images.

Clinical—T_2* maps were generated using a multi-echo gradient-echo pulse sequence with the following scan parameters: TE = 4, 10, 20, 30, 36, 42, 48, 54, 60, 67, 73, and 79 ms;

TR = 4000 ms; matrix size = 192 × 256; FOV = 200 × 200 mm; slice thickness 4 mm. T_2* maps were generated by fitting the signal intensity of the GRE images with a single monoexponential. For contrast-enhanced anatomical imaging, a T1 MP-RAGE sequence was used with the following scan parameters: TE = 3 ms, TR = 2300 ms, TI = 900 ms, matrix size 256 × 256 × 192, FOV= 256 × 256 × 192 mm. In each patient, the T_2* map obtained before $AscH^-$ treatment and 4 weeks after $AscH^-$ treatment were co-registered to the 4-week post-P-$AscH^-$ T_1+C images using an affine transformation. For ROI analysis, the contrast-enhancing lesions were manually segmented on the T_1+C images. Regions with necrosis, hemorrhage or post-surgical cavities were excluded from the analysis.

Image Analysis

Pre-clinical—T_2* maps were generated using a combination of 4 echo times (2.2 ms, 8.2 ms, 14.2 ms, 20.2 ms) and fitting each voxel to a mono-exponential curve using an in-house python code. For image registration, subsequent T_2-anatomical images were rigidly aligned to the initial T_2-anatomical image with the linear transformation matrix being applied to the associated T_2* map using Advanced Normalization Tools (ANTs) software. Images were imported to 3D Slicer software where regions of interest (ROIs) were delineated and mean T_2* values were calculated using the label statistics tool within 3D Slicer.

Clinical—T_2* maps were generated by fitting the signal intensity of the GRE images with a single monoexponential. In each patient, the T_2* map of the three-time points and FLAIR images were co-registered to the 4-h post-P-$AscH^-$ T_1+C images using an affine transformation (Fig. 1). For region-of-interest (ROI) analysis, the contrast-enhancing lesions and non-enhancing lesions were manually segmented on the T_1+C and FLAIR images, respectively. Contralateral normal-appearing white matter (cNAWM) was segmented on the T_1+C images using IBASPM: Individual Brain Atlases using Statistical Parametric Mapping Software (RRID:SCR_007110). Regions with necrosis, hemorrhage or post-surgical cavities were excluded from the analysis.

Phase 2 clinical trial design

A phase 2 clinical trial was conducted at the University of Iowa to evaluate the efficacy of combining pharmacological ascorbate with standard radiation and temozolomide in patients with newly diagnosed glioblastoma (GBM) patients including IDH mutant grade 4 astrocytoma. Approval was sought, and obtained, from the University of Iowa Institutional Review Board (Biomedical IRB-01; IRB 201211713). This phase 2 study was registered with clinicaltrials.gov (NCT02344355). The study was conducted according to ICH 3G(R2) as adopted by US law, the U.S. Common Rule, and the Belmont Report. All subjects provided independent, informed, written consent. Post-consent screening procedures included evaluating for glucose-6-phosphatase dehydrogenase deficiency as well as osmolarity tolerance by challenging the consented subjects with a 15-g test dose ascorbate infusion.

The study was broken into two phases: concomitant phase and adjuvant phase. Concomitant phase was defined as the time from day 1 of radiation until adjuvant cycle 1, day 1 and is similar to treatment paradigm put forth by Stupp et al.(2) In addition to the radiation

(61.2 Gy in 34 fractions) and temozolomide (75 mg m^{-2} daily, maximum of 49 days),(33) P-$AscH^-$ was infused three times weekly (87.5 g) as a maximum rate of 500 mL h^{-1}.

The adjuvant phase was the time from cycle 1 day 1 through end of cycle 6 or progression (whichever occurred first). Temozolomide was prescribed consistent with the Stupp regimen: 150 mg m^{-2} for days 1 through 5 of a 28-day cycle with a one-time escalation to 200 mg/m^2 in cycle 2 if the previous dose was well tolerated.(2) Pharmacological ascorbate infusions were given twice weekly (87.5 g). Use of tumor treating fields was prohibited but allowed upon completion of protocol directed therapy.

MGMT promoter methylation status on the GBM tumor tissue was determined by a PCR-based analysis at ARUP National Reference Laboratory (Salt Lake City, UT). IDH status was determined either immunohistochemically or next generation sequencing by the University of Iowa Hospitals and Clinics Clinical Histopathology Laboratory. Radiographic responses were assessed using RANO criteria evaluated by an independent neuroradiologist.(34)

Data sharing:

The data presented in this work was collected by the University of Iowa Department of Radiation Oncology Clinical Research Core and is available upon request of the corresponding author(s).

Results

The single-arm phase 2 clinical trial (NCT02344355) enrolled 55 subjects with analysis performed 12 months following the completion of treatment. Patient demographics are shown in Table 1. Study representativeness is described in Table S1. Overall survival (OS) and progression-free survival (PFS) were estimated with the Kaplan-Meier method and compared across patient subgroups with log-rank tests. Median OS was estimated to be 19.6 months (90% CI: 15.7 – 26.5 months) (Fig. 1A), a statistically significant increase compared to historic control patients (14.6 months).(2) This result also trends towards a significant increase in OS when compared to the 16 month OS observed by Stupp, et al. using temozolomide and RT alone.(35) While the current study was designed after the 2005 SOC regimen(2), the more modern comparison represents subjects who would have likely received relatively comparable salvage therapies.(35) Median PFS was 8.3 months (90% CI: 5.1 – 11.2 months), which was not significantly different from the historical control (6.9 months, Fig. 1B). Of this cohort, five subjects had tumors harboring an IDH mutation. These five subjects had a median PFS of 23.1 months and an OS of 53.1 months. This is consistent with increased survival associated with IDH mutant glioma tumors (median OS = 31 months).(36) These results provide encouraging evidence that P-$AscH^-$ may enhance the efficacy of chemo-radiation in GBM.

Following these encouraging clinical results, potential biomarkers associated with P-$AscH^-$ response were evaluated. O(6)-methylguanine methyltransferase (MGMT) is an enzyme that removes methylguanine and alkylguanine lesions directly and reverses the effects of DNA alkylating agents (e.g., temozolomide) (37,38). *MGMT* promoter methylation results

in epigenetic silencing and an impaired ability to remove the alkylation of DNA by temozolomide(39). Thus, *MGMT* promoter methylation is a traditional marker of GBM treatment response as patients with a methylated *MGMT* promoter (*MGMT* silent) have increased overall survival compared to patients with an unmethatyled *MGMT* promoter (median OS = 25.5 months vs. 12.4 months) (40,41). In the phase II trial, subjects with positive *MGMT* promoter methylation had a median OS = 26.5 months ($n = 26$) compared to 14.6 months ($n = 29$, $p<0.05$) for those with *MGMT* unmethylated tumors (Fig.1C). While patients with methylated MGMT promoters had improved survival when treated with P-AscH$^-$, TMZ and RT, these results were similar to those seen in historical patients treated with TMZ and RT alone. Thus, MGMT may not play a mechanistic role in or be a predictive biomarker for P-AscH$^-$ treatment response.

Based on our previous preliminary work suggesting T2* mapping can identify Fe oxidation state, T2* mapping was investigated as a mechanism-based, non-invasive biomarker of P-AscH$^-$ response (26). T_2* MRI (a surrogate Fe marker reported to acutely increase in the T_1-enhancing region of specifically GBM subjects 4 h after P-AscH$^-$ infusion(27)) was used to stratify GBM subjects for PFS and OS ($n = 49$; median T_2* = 50 ms). In the current study, no significant increase in T_2* relaxation time was observed following 4 weeks of P-AscH$^-$ therapy (Fig. 2A). No significant difference between tumor ROIs and the adjacent normal brain was observed prior to the beginning of treatment (Fig.S1), perhaps due to tumor variability in T_2* relaxation. This is consistent with previous data, which showed that P-AscH$^-$ did not change T_2* relaxation in normal appearing white matter acutely.(27) Interestingly, subjects with initial T_2* ≤ 50 ms (T_2*$_{low}$) demonstrated T_2* relaxation time increases following four weeks of P-AscH$^-$ therapy compared to subjects with initial T_2* > 50 ms (ΔT_2* (%) = +14.5 ± 6.5 % versus −4.2 ± 4.8 %, $p<0.05$; Fig. 2B). There was no significant difference in initial T_2* relaxation time in GBM tumors based on *MGMT* promoter methylation status (Fig. 2C). However, ΔT_2* was not significantly associated with OS (HR = 1.22, CI: 0.53 – 2.79, $p = 0.64$) or PFS (HR = 1.01, CI: 0.49 – 2.11, $p = 0.97$) using a Cox regression analysis. Therefore, while ΔT_2* metric may be reflective of an in vivo biochemical change, it may also be the result of a statistical regression to the mean phenomenon and requires further investigation.

For further evaluation of the utility of T_2* mapping a potential biomarker, the initial relaxation time was evaluated. T_2*$_{low}$ subjects were associated with a significant increase in PFS compared to T_2*$_{high}$ subjects (11.2 months vs. 5.7 months, $p < 0.05$, Fig. 2D). Estimated median OS in the T_2*$_{low}$ cohort trended higher (26.5 months) than the T_2*$_{high}$ cohort (17.5 months) but did not reach statistical significance ($p = 0.17$; Fig. 2E). When patients who did not receive P-AscH$^-$ therapy (*i.e.*, SOC alone), there was not a significant change in T_2* from baseline (Fig.S2A) nor was initial T_2* able to predict OS or PFS (Fig.S2B,C). These results are consistent with previous data showing that SOC was unable to alter T_2* relaxation times acutely.(27) These data support the hypothesis that low initial T_2*, indicative of high Fe^{3+}, may provide a novel predictive biomarker for predicting GBM subjects' responses to P-AscH$^-$.

Pre-clinical studies were designed to validate T_2* mapping as an Fe-sensitive technique capable of assessing P-AscH$^-$ sensitivity. For quality assurance, a test re-test study was

performed showcasing *in vivo* variability of T_2* mapping in normal mouse brains of ± 1 ms intra-scan and ≤ 3% inter-scan (Fig. S3A–C). In luciferized GBM (U87) tumors (Fig. 3A), seven-day treatment with P-AscH$^-$ significantly increased T_2* relaxation (45 ± 17 %) compared to contralateral normal brain tissue (−4.7 ± 6.0 %) (Fig. 3B,C, $p<0.05$) and untreated U87 tumors (Δ = 7.7 ± 6.1% *vs.* 43 ± 15%, $p<0.05$; Fig. 3D). Furthermore, the increased T_2* relaxation seen with 7 days of P-AscH$^-$ persisted for 4 days following a 3-day treatment break (Fig. 3E). These results support the hypothesis that persistent changes in $Fe^{2+/3+}$ induced by P-AscH$^-$ can be detected *in vivo* by T_2* mapping.

Alternatively, U251 GBM tumors treated with P-AscH$^-$ for 7 days showed no change in T_2* relative to baseline (28.7 ± 2.2 ms *vs.* 29.9 ± 1.9 ms, $p = 0.13$; Fig.3F). Consistent with our clinical trial results, innitial T_2* relaxation times were significantly longer in orthotopic U251 GBM, compared to U87 (29 ± 2 ms *vs.* 21 ± 1 ms; Fig. 3G), indicative of decreased iron content. P-AscH$^-$ induced T2* changes in U87 tumors were significantly greater than those observed in U251 tumors (Δ = 62.3 ± 15.9% *vs.* 5.0 ± 5.3%; Fig. 3H). Consistent with the hypothesis that T_2* can detect labile iron changes, U87 tumors had significantly more labile iron than U251 tumors following P-AscH$^-$ treatment (152 ± 8 μM *vs.* 126 ± 5 μM; Fig. 3I). Furthermore, in the responsive U87 tumor-bearing animals, the addition of P-AscH$^-$ to SOC was able to slow tumor growth following a 7 day treatment cycle (Fig.3J). Taken together, these pre-clinical data support the hypothesis that T_2* mapping detects redox-active Fe modulation *in vivo* to predict response to P-AscH$^-$.

Consistent with our *in vivo* data, U87 GBM cells exhibit significant sensitivity to P-AscH$^-$ leading to enhanced sensitivity to radiation and temozolomide while U251 were relatively resistant to P-AscH$^-$, resulting in no significant alterations in sensitivity to radiation and temozolomide (Fig. 4A,B). To model the hypothesis that intratumoral paramagnetic iron content, represented by decreased T_2* relaxation times, are prognostic of P-AscH$^-$ sensitivity, ferritin heavy chain (FtH) was overexpressed in U251 cells (U251 FtH+; Fig. S4). Ferritin is the primary enzyme responsible for iron storage, which is stored as the more paramagnetic Fe^{3+}.(42) Therefore, FtH overexpression is a useful model for the generation of a more paramagnetic cell. Consistent, with its role in iron storage, overexpression of FtH resulted in a significant decrease in redox active labile Fe^{2+} as evidenced by its ability to mitigate the effects of ferrous ammonium sulfate supplementation (Fig. 4C). FtH overexpression did not significantly alter the basal level of labile iron, which is likely due to lower basal levels of labile iron in U251 cells (Fig. S5). The iron sequestration effects of FtH overexpression were also reflected in T_2* mapping as relaxation times decreased demonstrating that the manipulation of intracellular Fe^{3+} can be detected with T_2* MRI (131 ± 4 ms *vs.* 114 ± 6 ms, Fig. 4D). In addition, U251 FtH+ cells showed increased expression of TfR and a 50% reduction in aconitase activity, suggesting an adaptive response reflective of decreasing labile Fe (Fig. S6A–C). Because P-AscH$^-$ can mediate the release of iron from Ft as labile Fe^{2+} (Fig. S7), it can be hypothesized that FtH overexpression should modulate P-AscH$^-$ sensitivity in a manner that is reflected in the endogenous T_2* relaxation time.(43–45) Based on the observed TfR overexpression, U251 FtH+ cells were treated with doxycycline and holo-transferrin (hTf), the substrate for TfR. In this iron metabolic model, a stepwise decrease in T_2* compared to control (range:84.2 ± 2.8 – 72.8 ± 3.9 ms; Fig. 4E) was observed, which is consistent with our previous results that

there is increased intracellular iron stored as Fe^{3+}. This combination significantly enhanced P-AscH$^-$ U251 clonogenic cell killing compared to P-AscH$^-$ alone (Fig. 4F). To further validate the translational potential of these data, the ability of P-AscH$^-$ to enhance radiation and temozolomide was tested in two patient-derived GBM cell lines (Fig. 4G). P-AscH$^-$ significantly enhanced the toxicity of radiation and temozolomide in GBM76 cells but not GBM06. Consistent with the previously observed pre-clinical and clinical results, GBM76 cells had a significantly shorter T_2* relaxation time than GBM06 cells (Fig.4H). Overall, these data support the overarching hypothesis that T_2* mapping can detect intracellular iron metabolic status and is a relevant prognostic marker for evaluating P-AscH$^-$ therapy responses.

Discussion

This study highlights two critical findings: 1. P-AscH$^-$ combined with radiation and temozolomide has the potential to significantly enhance GBM patient outcomes and 2. P-AscH$^-$ response can be evaluated using T_2* mapping. Targeting Fe metabolism using P-AscH$^-$ has shown significant promise in various clinical disease sites including pancreas cancer, non-small cell lung cancer, and glioblastoma(12,33,46,47). P-AscH$^-$ is believed to be a novel approach to target the aberrant Fe metabolic network in GBM tumors. This study further validates this as GBM patients receiving P-AscH$^-$ in combination with chemo-radiation have significantly improved clinical responses compared to historical control (median OS = 19.6 months versus 14.6 months). This represents a critical advancement in the clinical management of GBM tumors as this is the longest GBM median overall survival reported for phase II or III clinical trials.

In addition, this study showcased the biological and clinical utility of T_2* mapping. In this phase 2 trial, patients with more paramagnetic tumors (initial T_2* ≤ 50 ms) had improved clinical outcomes compared to subjects with less paramagnetic tumors (initial T_2* > 50 ms). This suggests that GBMs with higher baseline tumor iron content are more sensitive P-AscH$^-$ therapy. Mechanistically, P-AscH$^-$ is able to enhance GBM cell killing effects of temozolomide and radiation in an Fe-dependent manner as Fe chelation by deferoxamine diminished this effect(12). These data are supported by a previous study showing that increasing intracellular Fe content with Fe-sucrose can enhance colon cancer cell sensitivity to AscH$^-$(48). Consistent with these previous studies, genetically manipulating GBM cells to increase FtH expression leads to increased sensitivity to P-AscH$^-$. Furthermore, it has recently been reported that U251 GBM cells are unresponsive to P-AscH$^-$ enhancement of SOC *in vivo*; an effect that was overcome by the addition of iron oxide nanoparticles.(49) Thus, intratumoral iron appears to play a critical role in the utility of P-AscH$^-$ and GBM patients may benefit from the addition of iron supplementation to increase tumor Fe content prior to beginning P-AscH$^-$ therapy.

This study also showcased the biological relevance of T_2* oxidation state specificity. T_2* mapping was able to detect P-AscH$^-$ induced changes in labile iron *in vitro* in multiple GBM cell lines and using an *in vivo* orthotopic GBM model. However, the detectable changes in labile iron arising from T_2* oxidation state specificity only occurred in orthotopic GBM tumors with short initial relaxation times (U87). These results correlated with the

observations in human subjects as P-AscH$^-$ - mediated increases in T_2* relaxation occurred in initial T_2* relaxation times ≤ 50 ms and were directly reflected in the patient outcomes. These data further suggest that T_2* mapping can detect iron metabolic disruptions in a biologically and clinically relevant manner. Therefore, this study provides support for the biological and clinical relevance of a spin state-dependent theory of T_2* relaxation where relaxation times are largely derived from proton-electron dipole-dipole interactions allowing for the *in vivo* detection of the interconversion of $Fe^{3+} \leftrightarrow Fe^{2+}$ (26). Based on the prevalence of aberrant iron metabolic features in tumors and the interest in developing therapies to target this system, these data support the hypothesis that T_2* mapping can be broadly applied to evaluating the treatment responses of such approaches in across the spectrum of cancers.

In summary, the remarkable enhancement of efficacy seen in both OS and PFS by combining P-AscH$^-$ with chemo-radiation in this single arm, phase 2 clinical trial represents a major advance in the management of GBM. T_2* mapping appears to provide a novel non-invasive mechanism-based, iron-dependent biomarker that can predict outcomes to P-AscH$^-$ therapy. This robust pre-clinical mechanistic analysis of T_2* as a biomarker may enhance the broad utility of Fe-based MR imaging of metabolic perturbations during disease progression. Finally, the clinical deployment of T_2* mapping as an MRI technique may provide invaluable prognostic information allowing for the personalized management of Fe-dependent therapies and pathologies.

Supplementary Material

Refer to Web version on PubMed Central for supplementary material.

Acknowledgments:

The content is solely the responsibility of the authors and does not represent the views of the National Institutes of Health. The ESR facility at the University of Iowa provided invaluable support for the completion of this work. We would like to acknowledge Drs. Andrew Pieper, MD PhD and Edwin Vazquez- Rosa, PhD for their assistance in the establishment of our *in vivo* glioblastoma models. We acknowledge the Burke family for their financial support. We also acknowledge Gareth Smith for his assistance in the production of the figures and editing support. This work was supported by NIH grants T32 CA078586, P01 CA217797, P01 CA244091, R21 CA270742, and the Gateway for Cancer Research grant G-17-1500. Core facilities were supported in part by the Carver College of Medicine and the Holden Comprehensive Cancer Center, NIH P30 CA086862.

References

1. Wen PY, Kesari S. Malignant Gliomas in Adults. N Engl J Med. Massachusetts Medical Society; 2008;359:492–507.
2. Stupp R, Mason WP, van den Bent MJ, Weller M, Fisher B, Taphoorn MJB, et al. Radiotherapy plus concomitant and adjuvant temozolomide for glioblastoma. The New England journal of medicine 2005;352:987–96. [PubMed: 15758009]
3. Ostrom QT, Cioffi G, Waite K, Kruchko C, Barnholtz-Sloan JS. CBTRUS Statistical Report: Primary Brain and Other Central Nervous System Tumors Diagnosed in the United States in 2014–2018. Neuro-Oncology 2021;23:iii1–105. [PubMed: 34608945]
4. Schonberg DL, Miller TE, Wu Q, Flavahan WA, Das NK, Hale JS, et al. Preferential Iron Trafficking Characterizes Glioblastoma Stem-like Cells. Cancer Cell 2015;28:441–55. [PubMed: 26461092]

5. Keyer K, Imlay JA. Superoxide accelerates DNA damage by elevating free-iron levels. Proc Natl Acad Sci U S A 1996;93:13635–40. [PubMed: 8942986]
6. Breuer W, Shvartsman M, Cabantchik ZI. Intracellular labile iron. The International Journal of Biochemistry & Cell Biology 2008;40:350–4. [PubMed: 17451993]
7. Kruszewski M Labile iron pool: the main determinant of cellular response to oxidative stress. Mutation Research/Fundamental and Molecular Mechanisms of Mutagenesis 2003;531:81–92. [PubMed: 14637247]
8. Petronek MS, Spitz DR, Buettner GR, Allen BG. Linking Cancer Metabolic Dysfunction and Genetic Instability through the Lens of Iron Metabolism. Cancers (Basel) 2019;11:1077. [PubMed: 31366108]
9. Wardman P, Candeias LP. Fenton Chemistry: An Introduction. Radiation Research 1996;145:523–31. [PubMed: 8619017]
10. Qian SY, Buettner GR. Iron and dioxygen chemistry is an important route to initiation of biological free radical oxidations: an electron paramagnetic resonance spin trapping study. Free Radical Biology and Medicine 1999;26:1447–56. [PubMed: 10401608]
11. Petronek MS, Spitz DR, Allen BG. Iron–Sulfur Cluster Biogenesis as a Critical Target in Cancer. Antioxidants 2021;10 (9):1458. [PubMed: 34573089]
12. Schoenfeld JD, Sibenaller ZA, Mapuskar KA, Wagner BA, Cramer-Morales KL, Furqan M, et al. O2·− and H2O2-Mediated Disruption of Fe Metabolism Causes the Differential Susceptibility of NSCLC and GBM Cancer Cells to Pharmacological Ascorbate. Cancer Cell 2017;31:487–500.e8. [PubMed: 28366679]
13. Buettner GR, Jurkiewicz BA. Catalytic metals, ascorbate and free radicals: combinations to avoid. Radiat Res 1996;145:532–41. [PubMed: 8619018]
14. BIELSKI BHJ. Chemistry of Ascorbic Acid Radicals. Ascorbic Acid: Chemistry, Metabolism, and Uses [Internet]. AMERICAN CHEMICAL SOCIETY; 1982 [cited 2019 Dec 27]. page 81–100. Available from: 10.1021/ba-1982-0200.ch004
15. Schoenfeld JD, Sibenaller ZA, Mapuskar KA, Bradley MD, Wagner BA, Buettner GR, et al. Redox active metals and H2O2 mediate the increased efficacy of pharmacological ascorbate in combination with gemcitabine or radiation in pre-clinical sarcoma models. Redox Biology 2018;14:417–22. [PubMed: 29069637]
16. Anderson L, Holden S, Davis B, Prescott E, Charrier C, Bunce N, et al. Cardiovascular T2-star (T2*) Magnetic Resonance for the Early Diagnosis of Myocardial Iron Overload. European Heart Journal - Cardiovascular Imaging 2001;22:2171–9.
17. Henninger B, Kremser C, Rauch S, Eder R, Zoller H, Finkenstedt A, et al. Evaluation of MR imaging with T1 and T2* mapping for the determination of hepatic iron overload. European Radiology 2012;22:2478–86. [PubMed: 22645044]
18. Positano V, Salani B, Pepe A, Santarelli MF, De Marchi D, Ramazzotti A, et al. Improved T2* assessment in liver iron overload by magnetic resonance imaging. Magnetic Resonance Imaging 2009;27:188–97. [PubMed: 18667287]
19. Wood JC, Enriquez C, Ghugre N, Tyzka JM, Carson S, Nelson MD, et al. MRI R2 and R2* mapping accurately estimates hepatic iron concentration in transfusion-dependent thalassemia and sickle cell disease patients. Blood. 2005/04/28 ed. American Society of Hematology; 2005;106:1460–5.
20. Pierre TG St., Clark PR, Chua-anusorn W, Fleming AJ, Jeffrey GP, Olynyk JK, et al. Noninvasive measurement and imaging of liver iron concentrations using proton magnetic resonance. Blood 2005;105:855–61. [PubMed: 15256427]
21. Anderson LJ, Westwood MA, Holden S, Davis B, Prescott E, Wonke B, et al. Myocardial iron clearance during reversal of siderotic cardiomyopathy with intravenous desferrioxamine: a prospective study using T2* cardiovascular magnetic resonance. British Journal of Haematology John Wiley & Sons, Ltd; 2004;127:348–55. [PubMed: 15491298]
22. Carpenter J-P, He T, Kirk P, Roughton M, Anderson LJ, de Noronha SV, et al. On T2* magnetic resonance and cardiac iron. Circulation 2011/03/28 ed. 2011;123:1519–28. [PubMed: 21444881]

23. Rostoker G, Laroudie M, Blanc R, Griuncelli M, Loridon C, Lepeytre F, et al. Histological Scores Validate the Accuracy of Hepatic Iron Load Measured by Signal Intensity Ratio and R2* Relaxometry MRI in Dialysis Patients. J Clin Med MDPI; 2019;9:17. [PubMed: 31861625]
24. Langkammer C, Krebs N, Goessler W, Scheurer E, Ebner F, Yen K, et al. Quantitative MR Imaging of Brain Iron: A Postmortem Validation Study. Radiology. Radiological Society of North America; 2010;257:455–62.
25. Chavhan GB, Babyn PS, Thomas B, Shroff MM, Haacke EM. Principles, techniques, and applications of T2*-based MR imaging and its special applications. Radiographics. Radiological Society of North America; 2009;29:1433–49.
26. Petronek MS, St-Aubin JJ, Lee CY, Spitz DR, Gillan EG, Allen BG, et al. Quantum chemical insight into the effects of the local electron environment on T2*-based MRI. Scientific Reports 2021;11:20817. [PubMed: 34675308]
27. Cushing CM, Petronek MS, Bodeker KL, Vollstedt S, Brown HA, Opat E, et al. Magnetic resonance imaging (MRI) of pharmacological ascorbate-induced iron redox state as a biomarker in subjects undergoing radio-chemotherapy. Redox Biol 2020/11/19 ed. Elsevier; 2021;38:101804–101804. [PubMed: 33260088]
28. Mehdi Z, Petronek MS, Stolwijk JM, Mapuskar KA, Kalen AL, Buettner GR, et al. Utilization of Pharmacological Ascorbate to Enhance Hydrogen Peroxide-Mediated Radiosensitivity in Cancer Therapy. International Journal of Molecular Sciences 2021;22. [PubMed: 35008458]
29. Stookey L Ferrozine-A New Spectrophotometric Reagent for Iron. Anal Chem 1970;42.
30. Abbasi U, Abbina S, Gill A, Bhagat V, Kizhakkedathu JN. A facile colorimetric method for the quantification of labile iron pool and total iron in cells and tissue specimens. Scientific Reports 2021;11:6008. [PubMed: 33727584]
31. Case AJ, McGill JL, Tygrett LT, Shirasawa T, Spitz DR, Waldschmidt TJ, et al. Elevated mitochondrial superoxide disrupts normal T cell development, impairing adaptive immune responses to an influenza challenge. Free Radic Biol Med 2010/12/02 ed. 2011;50:448–58. [PubMed: 21130157]
32. OliverH Lowry, NiraJ Rosebrough, Farr AL, RoseJ Randall. PROTEIN MEASUREMENT WITH THE FOLIN PHENOL REAGENT. Journal of Biological Chemistry 1951;193:265–75. [PubMed: 14907713]
33. Allen BG, Bodeker KL, Smith MC, Monga V, Sandhu S, Hohl R, et al. First-in-Human Phase I Clinical Trial of Pharmacologic Ascorbate Combined with Radiation and Temozolomide for Newly Diagnosed Glioblastoma. Clin Cancer Res 2019/08/19 ed. 2019;25:6590–7. [PubMed: 31427282]
34. Wen PY, Chang SM, Van den Bent MJ, Vogelbaum MA, Macdonald DR, Lee EQ. Response Assessment in Neuro-Oncology Clinical Trials. JCO. Wolters Kluwer; 2017;35:2439–49.
35. Stupp R, Taillibert S, Kanner A, Read W, Steinberg DM, Lhermitte B, et al. Effect of Tumor-Treating Fields Plus Maintenance Temozolomide vs Maintenance Temozolomide Alone on Survival in Patients With Glioblastoma: A Randomized Clinical Trial. JAMA 2017;318:2306–16. [PubMed: 29260225]
36. Yan H, Parsons DW, Jin G, McLendon R, Rasheed BA, Yuan W, et al. IDH1 and IDH2 Mutations in Gliomas. N Engl J Med Massachusetts Medical Society; 2009;360:765–73. [PubMed: 19228619]
37. SHARMA S, SALEHI F, SCHEITHAUER BW, ROTONDO F, SYRO LV, KOVACS K. Role of MGMT in Tumor Development, Progression, Diagnosis, Treatment and Prognosis. Anticancer Res 2009;29:3759. [PubMed: 19846906]
38. Kitange GJ, Carlson BL, Schroeder MA, Grogan PT, Lamont JD, Decker PA, et al. Induction of MGMT expression is associated with temozolomide resistance in glioblastoma xenografts. Neuro-Oncology 2009;11:281–91. [PubMed: 18952979]
39. Hegi ME, Diserens A-C, Gorlia T, Hamou M-F, de Tribolet N, Weller M, et al. MGMT Gene Silencing and Benefit from Temozolomide in Glioblastoma. N Engl J Med Massachusetts Medical Society; 2005;352:997–1003. [PubMed: 15758010]

40. Annavarapu S, Gogate A, Pham T, Davies K, Singh P, Robert N. Treatment patterns and outcomes for patients with newly diagnosed glioblastoma multiforme: a retrospective cohort study. CNS Oncology. Future Medicine; 2021;10:CNS76.

41. Rivera AL, Pelloski CE, Gilbert MR, Colman H, De La Cruz C, Sulman EP, et al. MGMT promoter methylation is predictive of response to radiotherapy and prognostic in the absence of adjuvant alkylating chemotherapy for glioblastoma. Neuro-Oncology 2010;12:116–21. [PubMed: 20150378]

42. Harrison PM, Arosio P. The ferritins: molecular properties, iron storage function and cellular regulation. Biochimica et Biophysica Acta (BBA) - Bioenergetics 1996;1275:161–203. [PubMed: 8695634]

43. Badu-Boateng C, Pardalaki S, Wolf C, Lajnef S, Peyrot F, Naftalin RJ. Labile iron potentiates ascorbate-dependent reduction and mobilization of ferritin iron. Free Radical Biology and Medicine 2017;108:94–109. [PubMed: 28336129]

44. Moser JC, Rawal M, Wagner BA, Du J, Cullen JJ, Buettner GR. Pharmacological ascorbate and ionizing radiation (IR) increase labile iron in pancreatic cancer. Redox biology 2013;2:22–7. [PubMed: 24396727]

45. Badu-Boateng C, Naftalin RJ. Ascorbate and ferritin interactions: Consequences for iron release in vitro and in vivo and implications for inflammation. Free Radical Biology and Medicine 2019;133:75–87. [PubMed: 30268889]

46. Polireddy K, Dong R, Reed G, Yu J, Chen P, Williamson S, et al. High Dose Parenteral Ascorbate Inhibited Pancreatic Cancer Growth and Metastasis: Mechanisms and a Phase I/IIa study. Scientific Reports 2017;7:17188. [PubMed: 29215048]

47. Welsh JL, Wagner BA, van't Erve TJ, Zehr PS, Berg DJ, Halfdanarson TR, et al. Pharmacological ascorbate with gemcitabine for the control of metastatic and node-positive pancreatic cancer (PACMAN): results from a phase I clinical trial. Cancer Chemother Pharmacol 2013/02/05 ed. 2013;71:765–75. [PubMed: 23381814]

48. Brandt KE, Falls KC, Schoenfeld JD, Rodman SN, Gu Z, Zhan F, et al. Augmentation of intracellular iron using iron sucrose enhances the toxicity of pharmacological ascorbate in colon cancer cells. Redox Biol 2017/08/26 ed. Elsevier; 2018;14:82–7. [PubMed: 28886484]

49. Petronek MS, Teferi N, Caster JM, Stolwijk JM, Zaher A, Buatti JM, et al. Magnetite nanoparticles as a kinetically favorable source of iron to enhance GBM response to chemoradiosensitization with pharmacological ascorbate. Redox Biology 2023;62:102651. [PubMed: 36924683]

Statement of Translational Relevance:

P-AscH$^-$ combined with chemoradiation significantly increases GBM overall survival (19.6 months) as part of a phase II clinical trial compared to historical patients treated with chemoradiation, which can be predicted using T_2*-based MRI as an iron metabolic imaging technique.

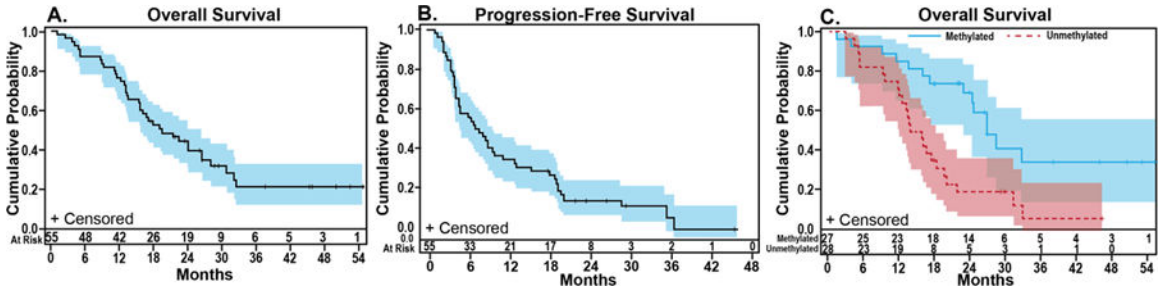

Figure 1. Encouraging patient outcomes in GBM subjects P-AscH^{-}.

A. Median OS was 19.6 months (90% CI: 15.7 – 26.5 months) analyzed using the Kaplan-Meier method. **B.** Median PFS was 8.3 months (90% CI: 5.1 – 11.2 months). **C.** Patients with unmethylated disease had significantly poorer OS (median = 14.6; 95% CI: 11.7 – 18.0) compared to those with methylated disease (median = 26.5; 95% CI: 22.5 – Not Reached, $p<0.05$).

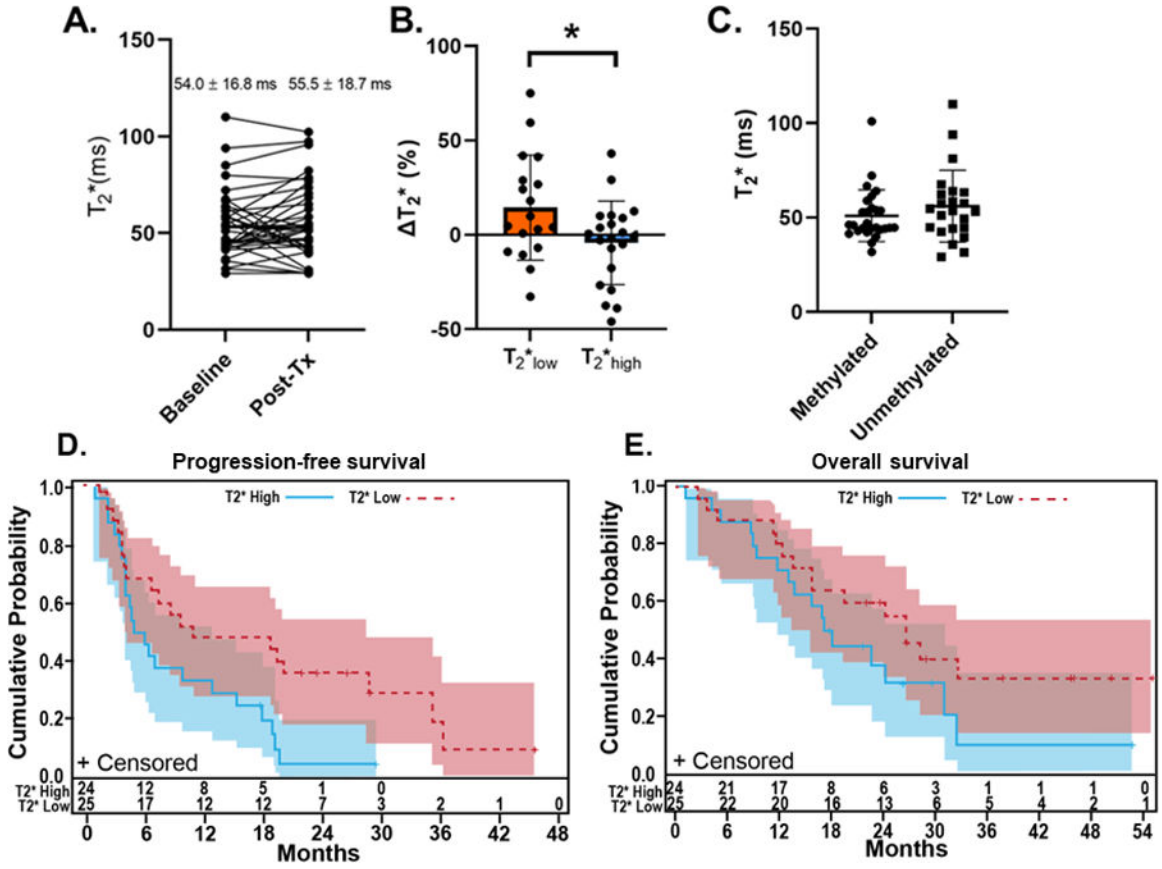

Figure 2. T_2* mapping predicts enhancement of outcomes of glioblastoma in human subjects treated with P-AscH$^-$.

A. Comparison of baseline T_2* relaxation time to post P-AscH- relaxation time following 4-weeks of therapy. Values represent the cohort mean at that time point ± SD. **B.** Comparison of change in T_2* relaxation time (%) following 4 weeks of P-AscH$^-$ + SOC therapy for subjects in the "low" relaxing cohort ($T_2*_{initial} \leq 50$ ms) compared to "high" relaxing cohort ($T_2*_{initial} > 50$ ms). *$p<0.05$ using a Welch's T-test. **C.** Mean initial T_2* relaxation time for subjects with methylated and unmethylated promoter regions. *$p<0.05$ using an unpaired, Welch's T-test. **D.** T_2*_{high} (median = 5.7;95% CI: 4.2 – 13.0 mos.) patients had worse progression-free survival compared to T_2*_{low} patients (median = 11.2; 95% CI: 4.4 – 28.5 mos., $p<0.05$). **E.** A statistically significant difference between T_2*_{high} (median = 17.5; 95% CI: 11.7 – 30.9 mos.) and T_2*_{low} (median = 26.5; 95% CI: 15.5 – Not Reached mos.) in terms of OS was not evidenced ($p=0.17$).

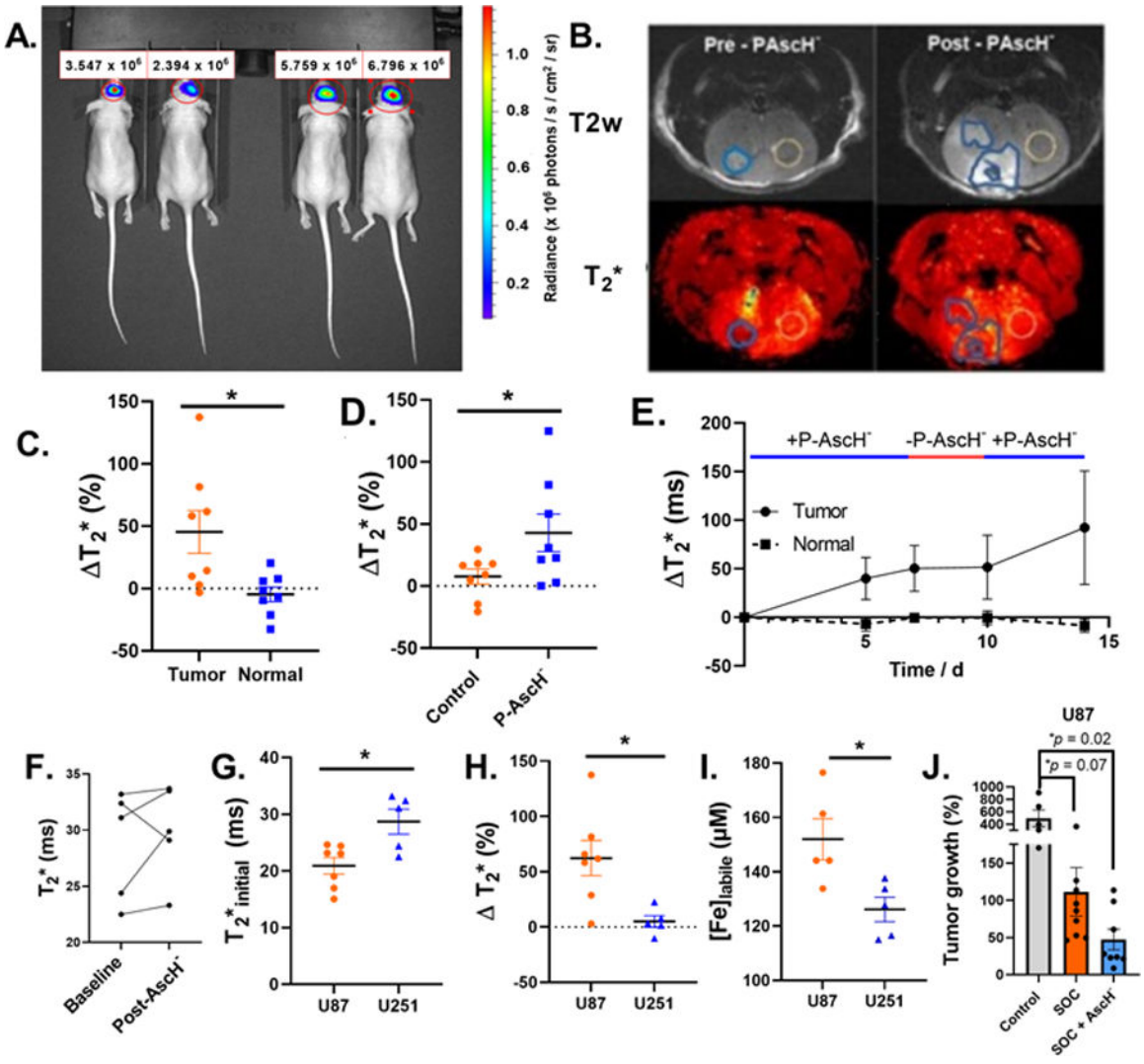

Figure 3. T_2* detects P-AscH$^-$ - induced iron metabolic changes in an orthotopic GBM model.

A. One week following tumor cell implantation, U87 cells that had been transduced with firefly luciferase were monitored with bioluminescent imaging to confirm the presence of tumor. **B.** Nu/J athymic mice with orthotopically implanted GBM tumor cells were treated with pharmacological doses of AscH- (4 g kg-1 twice daily) to evaluate the in vivo effects of iron metabolic changes on T2* relaxation times. Upper Panels: Tumor regions of interest (ROI) are defined by a hyperintense region on a T2 – weighted (T2w) anatomical image (blue) with regions of hemmorage excluded and normal tissue are defined by a 1 mm diameter cylinder spanning the length of the tumor on the contralateral side (yellow). Lower Panels: Representative T2* mapping image outputs. Mean ROI T2* relaxation times are determined using the Label Statistics image quantification package 3DSlicer software. **C/D.** ΔT_2* (%) in U87 tumors relative to adjacent, contralateral normal tissue (**C**) and untreated U87 tumors **(D)** following 7 days of P-AscH$^-$ treatment. Error bars represent SEM with *p<0.05 using a paired, two-tailed Welch's T-test. **E.** Time-dependent ΔT_2* ($\Delta = T_2{*}_{treatment} - T_2{*}_{initial}$) by P-AscH- where treatment was halted from day 7–10. Error bars represent SEM (n = 5–8). **F.** Mean T2* relaxation times of orthotopically implanted U251 GBM

tumors following 7 days of P-AscH- (4 g kg-1 twice daily) treatment. p = 0.45 using a paired, two-tailed, Welch's T-test. **G/H/I.** Baseline T2* (**G**), ΔT2* (%, **H**), and Labile Fe content (**I**) in U87 and U251 tumors following 7-day treatment with P-AscH^{-}. Error bars represent SEM with *p<0.05 using a paired, two-tailed Welch's T-test. **J.** Changes in MRI tumor volume (%) following a one-week cycle of treatment consisting of untreated controls (n =5), SOC (12 Gy x 1 radiation + 2.5 mg TMZ, n = 9) ± daily 4 g kg^{-1} P-AscH^{-} (n = 7). *p<0.05 using a one-way ANOVA with a post-hoc Tukey's test for multiple comparisons.

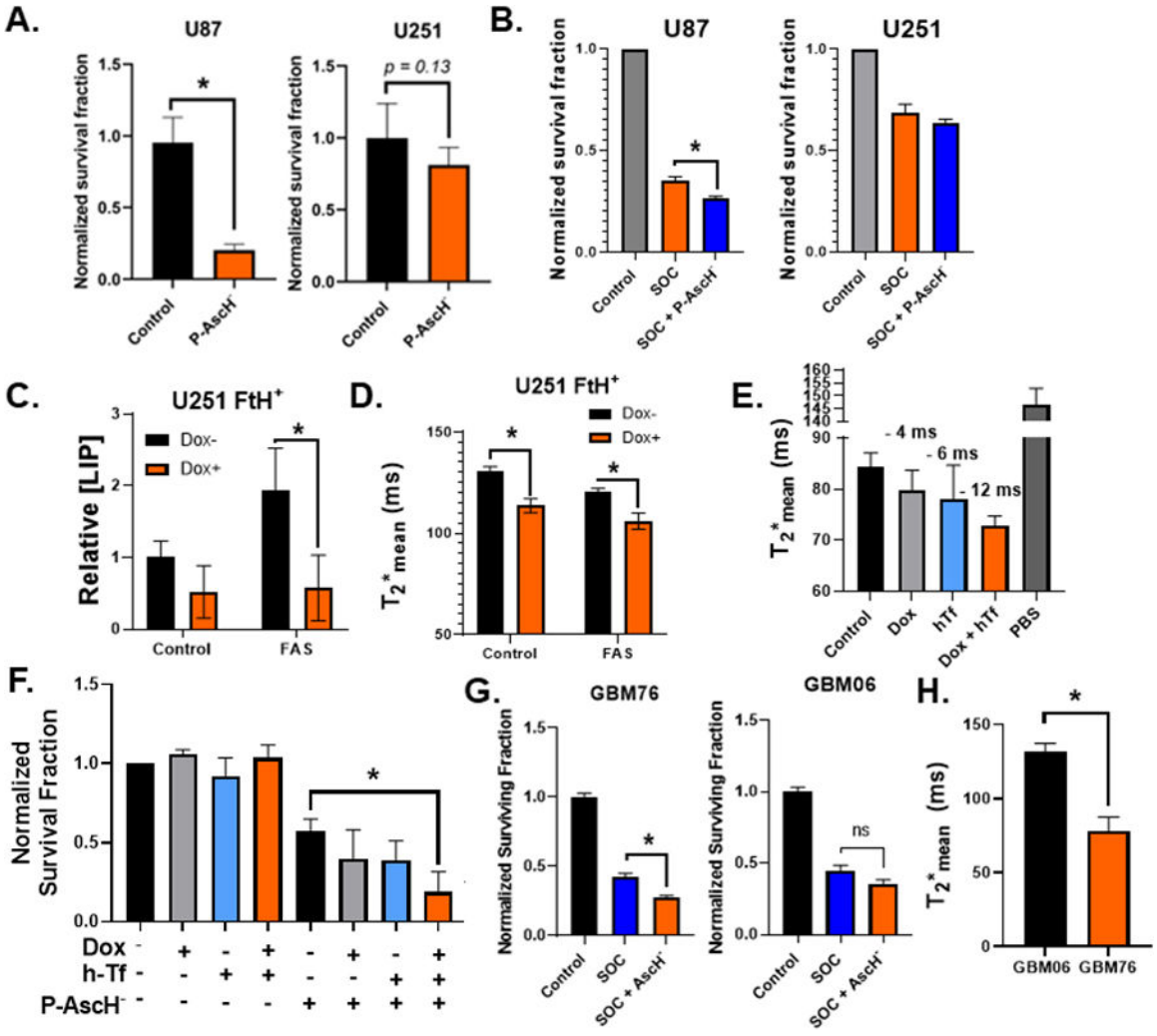

Figure 4. T_2* mapping reflects labile iron modulation to predict P-AscH$^-$ sensitivity.

A. Clonogenic survival analysis of U87 and U251 treated for 1 h with P-AscH$^-$ (20 pmol cell^{-1}; range: 6–8 mM). Error bars represent mean ± SEM of 2–3 independent experiments performed with 3–6 technical replicates. *$p < 0.05$ using an unpaired, Welch's T-test. **B.** Clonogenic survival analysis of U87 and U251 cells following treatment of standard of care (SOC) therapy (1 h SOC = 2.5 mM temozolomide and 2 Gy radiation) ± P-AscH$^-$ (1 h,10 pmol cell^{-1}). Error bars represent SEM (n = 2–3 independent experiments) with *p<0.05 using a Welch's T-test comparing treatment groups. **C/D.** Labile iron (B) and T2* (C) measures of U251 FtH+ cells treated with doxycycline (1 μg mL^{-1}, 48 h) ± 80 μM FAS (3 h). Changes in labile iron were measured using the iron sensitive calcein-AM flow cytometry probe and evaluating FITC fluoresence changes. Error bars represent mean ± SD with *p<0.05 using a two-way ANOVA with a post-hoc Tukey's test for multiple comparisons. **E.** T_2* in U251 FtH+ cells following 72 h dox treatment (1 μg mL^{-1}) ± holo-Tf supplementation (200 μg mL^{-1}). **F.** Clonogenic survival of U251 FtH+ ±dox (1 μg mL^{-1}, 72 h) ± holo-Tf supplementation (200 μg mL-1) ± P-Asc$^-$ (1 h, 20 pmol cell^{-1}; ≈ 10 mM). Error bars represent mean ± SEM (n = 3–5) with *p<0.05 using a one-way ANOVA test with a post-hoc Tukey's multiple comparison test of all treatment groups. **G.** Clonogenic

survival analysis of GBM76 and GBM06 cells following treatment of standard of care (SOC) therapy (1 h SOC = 2.5 mM temozolomide and 2 Gy radiation) ± P-AscH^{-} (1 h,10 pmol cell^{-1}). Error bars represent SEM (n = 3 independent experiments) with *p<0.05 using a one-way ANOVA with a post-hoc Tukey's test comparing individual treatment groups. **H.** Baseline T_2* measures in GBM06 and GBM76 cells. Error bars represent SEM (n = 6) with *p<0.05 using a Welch's T-test.

Table 1.

Patient demographics.

Variable	Level	N = 55 (%)
Gender	F	24 (43.6)
	M	31 (56.4)
Race	White	54 (98.2)
	Unknown	1 (1.8)
Ethnicity	Hispanic or Latino	1 (1.8)
	Non-Hispanic	54 (98.2)
IDH	Mutated	5 (7.7)
	WT	48 (92.3)
	Unidentified	2
MGMT	Methylated	27 (49.1)
	Unmethylated	28 (50.9)
Progression	No	15 (27.3)
	Yes	40 (72.7)
Status	Alive	17 (30.9)
	Dead	38 (69.1)
[a]Extent of Resection	Biopsy	6 (10.9)
	Subtotal resection	36 (65.4)
	Gross-total resection	13 (23.6)

[a]Defined by T_1-enhancing lesion on MRI.